Arch. Metall. Mater. **70** (2025), 2, 819-828

DOI: https://doi.org/10.24425/amm.2025.153484

M. ALI I. ALWAKWAK[1], I. ESEN[1*], H. AHLATCI[2], E. KESKIN[2]

EFFECTS OF YTTRIUM AND LANTHANUM ELEMENTS ON THE MICROSTRUCTURE AND WEAR BEHAVIOUR OF MAGNESIUM

This research investigates the impact of yttrium and lanthanum reinforcement on the dry wear, friction, and microstructure of magnesium alloy. The research investigates the effects of the processes such as as-casting and post-homogenization. The alloys MgY3.21La3.15 and MgY4.71La3.98 were created using a process of controlled melting and casting in an atmosphere-controlled environment. The MgY3.21La3.15 alloy, after undergoing homogenization, has a maximum hardness of 93.70 HB from 81.61 HB for the as- cast alloy. The MgY3.21La3.15 alloy exhibits a weight reduction of 0.024 g and a wear rate of 2.44×10^{-6} g/Nm, which demonstrates exceptional resistance to wear. The MgY4.71La3.98 alloy exhibits a weight loss of 0.053 g and a wear rate of 5.3×10^{-6} g/Nm. Friction occurs in parallel due to wearing, thus the MgY3.21La3.15 alloy has the lowest friction coefficient with 0.090.

Keywords: Mg; Yttrium; Lanthanum; Microstructure; Tribological behaviour

1. Introduction

Magnesium alloys have garnered significant interest as a potentially valuable lightweight material [1-3]. In recent years, there has been a notable surge in research and development endeavours cantered on magnesium and its alloys. The increasing recognition of the importance of reducing the weight of transportation vehicles has been cited as the reason for this phenomenon [4-6]. Magnesium alloys have been found to have inadequate tribological characteristics [7]. Magnesium alloys are highly effective in automotive applications that involve non-lubricated wear. They can effectively replace various components such as brakes, gear arrangements, and steering mechanisms. During this process, component losses occur as a result of dynamic friction. The continuous sliding motion generates frictional force, which impacts the tribological behavior of these components [8]. Considerable research has been conducted to overcome these challenges in magnesium alloys by modifying their chemical composition, employing plastic deformation techniques (such as extrusion, rolling, or forging), and applying heat treatments. These efforts aim to improve the tribological properties of magnesium alloys [9-14]. The addition of rare earth (RE) elements to magnesium has proven to be a successful approach in achieving a balance between strength and ductility. Recent studies have shown that this approach improves grain refinement, aging response, and the formation of high melting point secondary phase particles [15-23]. The solubility of rare earth elements in magnesium alloys has been used as an indicator of their impact. Elements with low solubility in the magnesium (Mg) matrix have negligible influence on the strength of both the solution and the precipitate. The excessive presence of elements in magnesium alloys has resulted in notable alterations in their microstructure, ductility, and strength properties. This phenomenon arises when excess elements undergo reactions with other alloying elements, leading to the creation of particles that contain rare earth elements (RE). The particles containing Re contribute to the increased strength of the secondary phases [13]. Mg-RE alloys exhibit a diverse range of phases, such as $Mg_{12}RE$, $Mg_{17}RE_2$, Mg_3RE, or Mg_2RE [24]. Therefore, it is crucial to accurately describe the microstructure to better understand the impact of rare earth elements (RE) on the tribological properties of magnesium alloys. Numerous studies have been conducted worldwide to examine the effects of different rare earth (RE) additions on the microstructural and mechanical properties of magnesium (Mg) alloys [25-30]. The wear behavior of Mg-RE alloys has been insufficiently studied. Extensive research has been

[1] KARABUK UNIVERSITY, MECHANICAL ENGINEERING DEPARTMENT KARABUK 78050, TURKEY
[2] KARABUK UNIVERSITY, METALLURGICAL AND MATERIALS ENGINEERING DEPARTMENT, KARABUK 78050, TURKEY
* Corresponding author: iesen@karabuk.edu.tr

conducted on the wear characteristics of ternary and quaternary Mg-RE alloys. Prasad et al. [8] examined the effects of a small amount of La on the wear properties of the Mg-10Dy alloy. The study revealed a significant reduction in wear rate for the alloy containing La when compared to the Mg-10Dy alloy. Yarkadas et al. [31] investigated the mechanical and wear properties of Mg-3Al-3Sn-3Sb alloy with varying weight percentages (1%, 3%, and 5%) of La. They found that the wear rates were low in La-containing alloys. Nouri et al. [32] examined the effects of yttrium on the wear, corrosion, and corrosive wear properties of Mg-3%Al alloy. The researchers noted that the addition of yttrium led to improved wear resistance. Zafari et al. [33] observed an improvement in wear resistance with the addition of 1.2% and 3% lanthanum by weight to the AZ91 alloy. Banijamali et al. [34] found that adding the Y element to the ZK60 extruded alloy led to a reduction in wear rate and friction coefficient. In a study conducted by Hamdy [35], the investigation focused on the wear resistance of an Al-Cu-Mg alloy with the addition of yttrium (Y), erbium (Er), and zirconium (Zr). The results indicated that the inclusion of yttrium (Y) led to an enhancement in wear resistance.

Understanding the tribological properties of a material is essential for predicting its durability and identifying possible modes of failure [36]. Scientists generally agree that the tribological properties of magnesium alloys need enhancement to meet the demands of various industries. While previous studies have investigated the impact of various rare earth elements on the properties of magnesium alloys, limited research has focused on the effects of minor alterations in the rare earth composition of cast and homogenized magnesium alloys on these characteristics. This study aims to investigate the impact of varying amounts of lanthanum and yttrium on the microstructure and tribological properties of magnesium alloys.

2. Materials and methods

Following the casting process, the chemical composition of the alloys was determined by weight using X-ray fluorescence (XRF Rigaku ZSX Primus II, Japan), while the phases generated in the alloy were determined using X-ray diffractometry (XRD Rigaku Ultima IV, Japan). TABLE 1 presents the chemical compositions of two alloys, namely MgY3.21La3.15 and MgY4.71La3.98.

TABLE 1

Alloy compositions (wt.%)

Alloy	Constituent Chemicals (wt.%)			
	Y	La	Zr	Mg
MgY3.21La3.15	3.216	3.151	0.626	Bal.
MgY4.71La3.98	4.715	3.984	1.163	Bal.

Firstly, to melt and cast the alloys, a low-pressure system was employed, which was regulated by the atmosphere. The ingots of magnesium purified to 99.9% were added to the ladle. To avoid leakage, thermal insulation double and O-ring are mounted on the melting furnace top cover to measure its interior temperature. The crucible was filled with the primary components and alloys in estimated proportions at a temperature of 780°C. The mixture was then stirred for a duration of 15 minutes. Mg-30La and Mg-30Y are master alloys containing rare earth elements. Then, the melt was combined with the 200°C-heated master Mg-30Zr alloy. The melting furnace used CO2+ 0.8 SF6 shielding gas to isolate the crucible from the environment. A metal pipe was submerged in the melt after being heated to 700°C in a separate furnace. At 300 degrees Celsius on the pipe, the cylindrical mold was filled with 2 bars of pressure.

The eutectic transition temperature of the Mg-Y alloy was determined to be 566°C, [37] which is in close proximity to the phase breakdown temperature of the alloy system. In contrast, the eutectic transition temperature of the Mg-La alloy was found to be 548°C [38]. To accomplish thorough homogenization without excessive heating, the homogenization temperature for the alloy was deliberately established in a range of 5-10°C below the solidus curves. In practice, a greater homogenization temperature reduced homogenization time, increased production efficiency, and provided good homogeneity. 525°C homogenized. The ingot castings, which were wrapped with aluminum foil, were subjected to a temperature of 525°C for a duration of 8 hours in a sand mixture consisting of SiO2 and graphite. The alloys underwent a process of homogenization in the furnace, followed by rapid cooling in water. The alloys' microstructure was studied after casting and homogenization using a picral etching solution composed of 6 g of C6H3N3O7, 5 ml of CH3COOH, 10 ml of pure H2O, and 100 ml of C2H6O. Optical microscope (LOM-Carl Zeiss light optical microscope) was used to see the change of grains in phase structure; electron microscope (SEM- Carl Zeiss Ultra Plus scanning electron microscope) and EDX (energy dispersion X-ray spectrometry) were investigated to reveal the secondary phases. The Brinell hardness was determined by employing 2.5 mm steel balls under a load of 187.5 N.

In order to determine the tribological properties, wear and friction properties were examined. Samples with 3/4 cylindrical surfaces, 16 mm in diameter and length, were made for the device's sample bed to conduct wear testing. The surfaces intended for wear were abraded using sandpaper with a grit size of up to 1200 μm. The weights of the samples, which were cleaned using ethanol, were then measured using a Precisa brand balance with a precision of 0.1 mg. Abrasion experiments were conducted using a back and forth wear testing apparatus under dry conditions. The applied load was 20 N, the sliding velocity was 0.1 m/s, and the total sliding distance was 10000 m. AISI 52100 quality high-hardness steel ball is used as the abrasive tip material. In order to remove wear residues, the sample surface was periodically cleansed using ethanol at intervals of 2000 meters. The weight measurements of the samples that underwent cleaning with ethanol were conducted using precision balances and thereafter subjected to the back-and-forth abrasion test once again. By using these values, the weight losses depending on the distance

were found by subtracting the post-wear value from the pre-wear value. The data pertaining to mass loss was transformed into a specific wear rate through the utilization of Eq. (1).

$$\text{Specific Wear Rate}\left(\text{g / N.m}\right) = \\ = \frac{\text{Wear Mass Loss}\left(\text{g}\right)}{\text{Applied Load}\left(\text{N}\right)\times\text{Sliding Distance}\left(\text{m}\right)} \quad (1)$$

The friction coefficient was calculated according to the Eq. (2) given below, according to Coulomb's law of friction. In the equation; F_S defines the friction force, F_N defines the test load, μ the friction coefficient.

$$\mu = \frac{F_S}{F_N} \quad (2)$$

The measurement of the friction force throughout the wear process was conducted by connecting a load cell to the tribometer arm, and the resulting data was promptly recorded on the computer. Depending on the changing alloy element amount and wear load after the wear test, the wear mechanism was investigated by means of SEM and EDX devices.

3. Results and discussion

3.1. XRD Patterns

The X-ray diffraction (XRD) analysis of the MgY3.21La3.15 alloy primarily reveals the presence of the $Mg_{24}Y_5$ phase, which is characterized by a high yttrium content. Conversely, in the MgY4.71La3.98 alloy, the XRD analysis indicates the presence of the MgY phase. Furthermore, it is worth noting that the X-ray diffraction (XRD) standard cards commonly exhibit prominent peaks corresponding to the $LaMg_3$ phase in both alloys. Mg_2Y and La_2Mg_{17} phases appeared as the initial XRD peaks at 17° (Fig. 1(a) in MgY3.21La3.15 alloy. The diffraction patterns obtained from the samples of α-Mg, $Mg_{12}La$, and La_2Mg_{17} exhibited distinct peaks at an angle of 14°, as seen in Fig. 1(b) (MgY4.71La3.98). Conversely, the peaks corresponding to $Mg_{12}La$ and Mg_2Y were observed at an angle of 17°. The X-ray diffraction (XRD) investigation revealed that the peak intensity in both alloys was detected at an angle of 36.5 degrees. MgY3.21La3.15 alloy has α-Mg, Mg_2Y, $Mg_{24}Y_5$, $Mg_{12}La$, and La_2Mg_{17} phases, whereas MgY4.71La3.98 alloy contains α-Mg, $Mg_{12}La$, and La_2Mg_{17} phases. In Fig. 1(a), the XRD peaks of MgY3.21La3.15 alloy finish at 82° degrees, with the $LaMg_3$ phase; in Fig. 1(b), the XRD peaks of MgY4.71La3.98 alloy terminate at 85° degrees, with the $LaMg_3$ and La_2Mg_{17} phases.

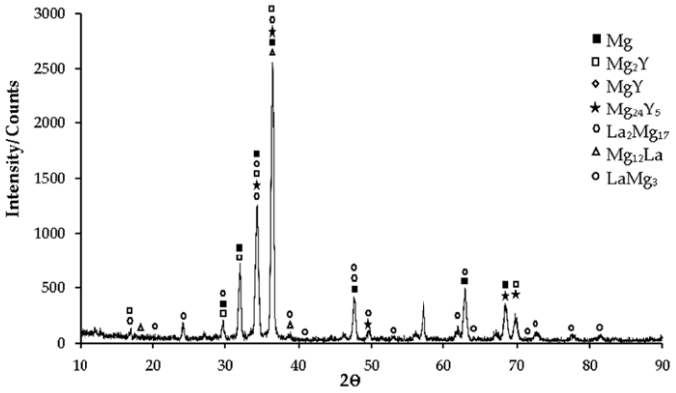

(a)

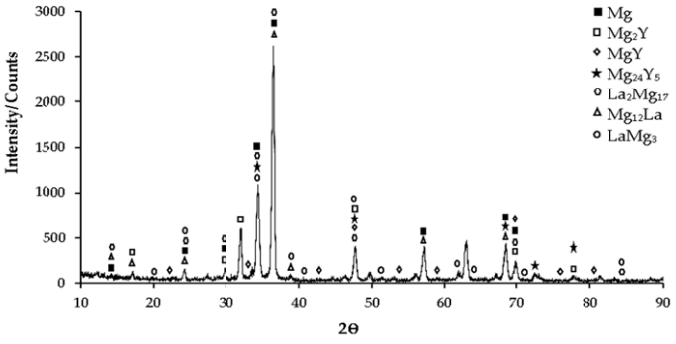

(b)

Fig. 1. X-ray diffraction (XRD) patterns of after-cast alloy: (a) MgY3.21La3.15, and (b) MgY4.71La3.98

3.2. Microstructure

LOM pictures of as-cast MgY3.21La3.15 and MgY4.71 La3.98 alloys are shown in Figs. 2(a) and 2(b). There are three-phase structures in microstructures. This group encompasses eutectic compounds with a reticular structure, together with α-Mg phases that have a lamellar shape. The presence of eutectic compounds was predominantly noted in the immediate vicinity of the grain boundaries of the α-Mg crystals, whereas the lamellae-like phases displayed a more homogeneous dispersion inside the crystals. The X-ray diffraction (XRD) patterns shown in Figs. 1(a) and 1(b) reveal that the peaks associated with the eutectic phases extend toward the borders of the grains. This observation suggests the existence of intermetallic compounds have consisted of α-Mg and $Mg_xRE(La/Y)_y$ inside the material. With a rise in La content, the eutectic phase consisting of α-Mg and $Mg_{17}L_{a2}$ demonstrated a phenomenon of lamellae structure coarsening. With a rise in La content, the eutectic phase consisting of α-Mg and $Mg_{17}La_2$ demonstrated a noticeable has been coarsened of its lamellae structure [39]. The presence of yttrium resulted in an augmentation of dendrite-like phase structures and network structures at the grain boundaries [40]. Following homogenization heat treatment, MgY3.21La3.15 and MgY4.71La3.98 alloys were observed under an optical microscope in Figs. 3(a) and 3(b). The homogenization procedure has resulted in a reduction in the occurrence of lamellae-like phases inside the interior regions of α-Mg granules, hence promoting the uniform distribution of alloy elements across the whole alloy system. According to Zhang et al. [41], it has been suggested that the presence of the $Mg_{24}Y_5$ phase decreases at the grain borders after the process of homogenization. On the other hand, Guo et al. [42] propose that the $LaMg_{12}$ phase surrounds and isolates the α-Mg grains.

Figs. 4(a) and 4(b) depict SEM micrographs of as-cast MgY3.21La3.15 and MgY4.71La3.98 alloys. TABLE 2 presents the results of the Energy Dispersive X-ray (EDX) study conducted on the second phase, which exhibits different morphologies denoted as (A-F) in Fig. 4(a)-(b). The Y and La phases have undergone dissolution inside the α-Mg matrix at position A in the as-cast MgY3.21La3.15 alloy, as seen in Fig. 4(a). At point B, it is hypothesized that the $Mg_{24}Y_5$ phase, which is rich in yttrium, has a rectangular or elliptical shape, consistent with Ref. [43]. This phase is characterized by a light gray contrast color observed at both the grain and grain borders, as indicated by the Energy Dispersive X-ray Spectroscopy (EDX) analysis (refer to Table 2). Grain structures in $LaMg_3$ are cube-shaped at the C location (Fig. 4(a)). In as-cast MgY4.71La3.98 alloy, the phase shown in Fig. 4(b) has been identified as La_2Mg_{17} based on the percentage of La content. This identification was made by analysing the bright white contrast-colored ellipse and rod-like intermetallics present in the grain structure at the D point, as shown in the EDX analysis presented in TABLE 2. It's possible that the little cube-shaped white structures at E's grain and grain borders are $Mg_{24}Y_5$ and $LaMg_3$ intermetallics. Magnesium-rich $Mg_{12}La$ and Mg_2Y intermetallics may exist at the F point, as predicted by the almost identical La%, Y% elemental ratios. Figs. 5(a) and 5(b) depict SEM micrographs of homogenized MgY3.21La3.15 and MgY4.71La3.98 alloys. TABLE 3 presents the results of the Energy Dispersive X-ray (EDX) investigation conducted on the second phase, which exhibits various morphologies as indicated by labels (A-F) in Fig. 5(a)-(b). In homogenized MgY3.21La3.15 alloy, as shown in Fig. 5(a), the grain boundaries have been located at the A point exhibiting a high density of intermetallics. These intermetallics have characterized by their small size and cubic morphology. Furthermore, with the presence of these structures at the borders between grains, there are also rectangular structures within the individual grains. It is believed that $Mg_{24}Y_5$ and $Mg_{12}La$ are the intermetallics detected in the XRD patterns (Fig. 1(a)) for the intermetallics discovered here. Furthermore, the presence of elongated structures inside the grain at point B, together with the vascular white contrast, has garnered interest. These structures have been hypothesized to consist of Mg_2Y and $LaMg_3$. The el-

(a)

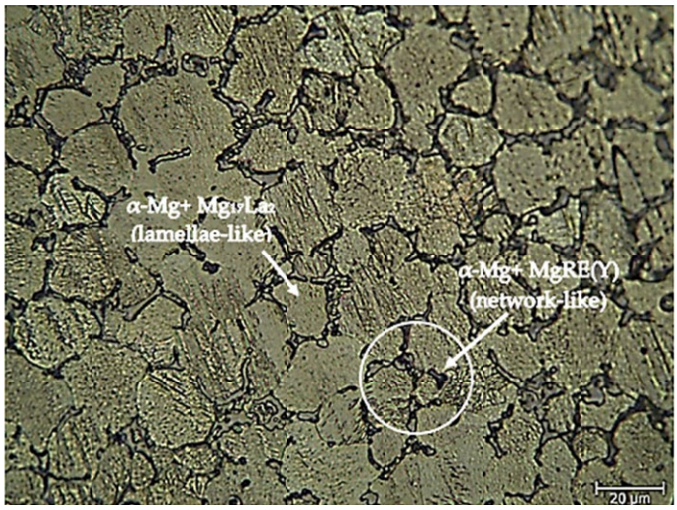

(b)

Fig. 2. Image of after-cast alloy LOM (50X): (a) MgY3.21La3.15 and (b) MgY4.71La3.98

(a)

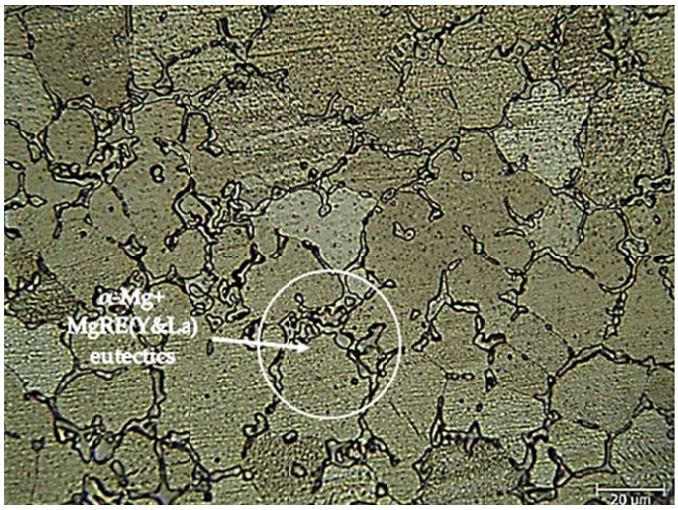

(b)

Fig. 3. Image of homogenized alloy LOM (50X): (a) MgY3.21La3.15 and (b) MgY4.71La3.98

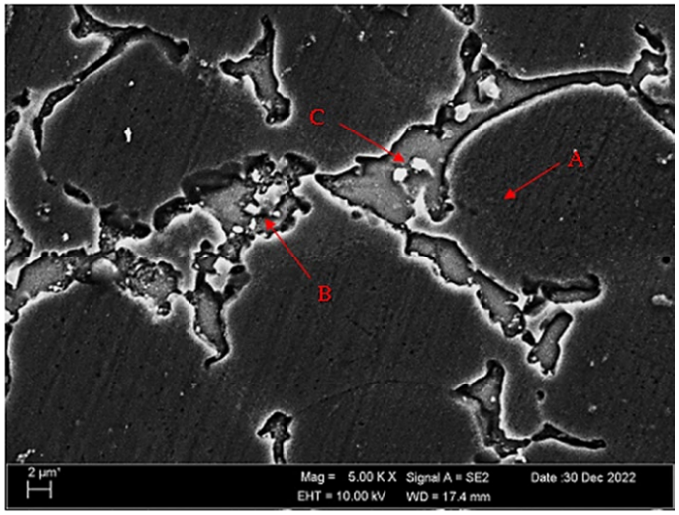

(a)

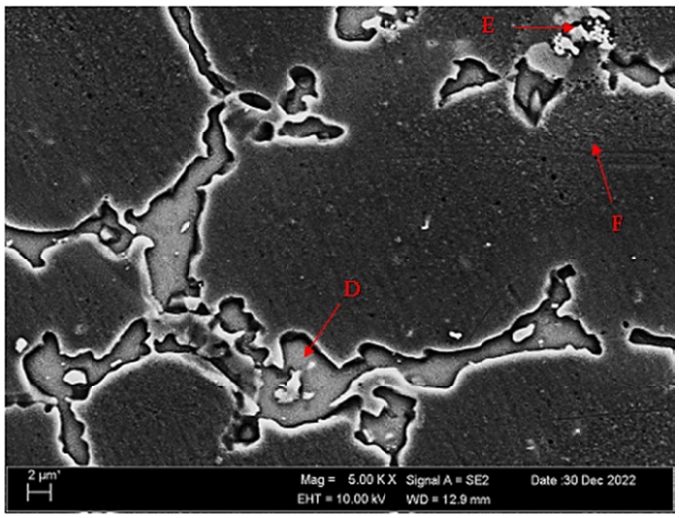

(b)

Fig. 4. Image of after-cast alloy SEM: (a) MgY3.21La3.15 and (b) MgY4.71La3.98

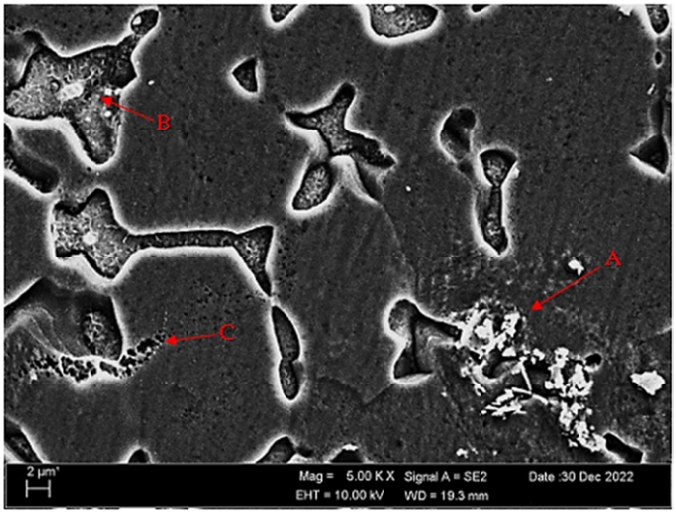

(a)

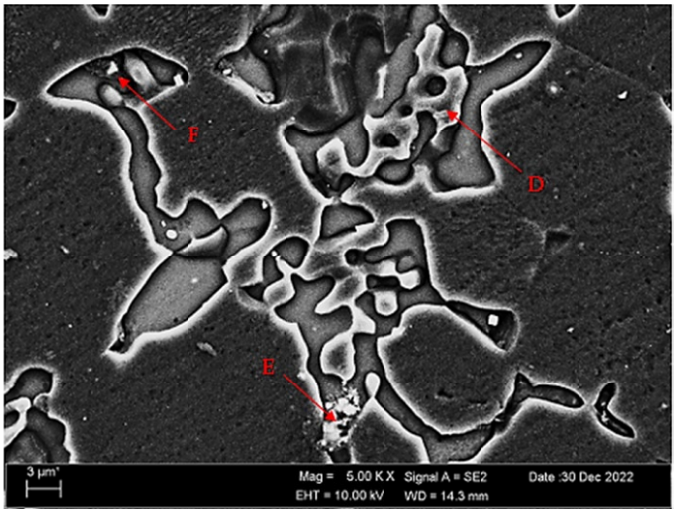

(b)

Fig. 5. Image of homogenized alloy SEM: (a) MgY3.21La3.15 and (b) MgY4.71La3.98

liptical structure seen at point C, characterized by a contrasting white grain, has likely attributed to the presence of the Mg_2Y intermetallic compound. Dendritic rod-like structures had seen at the D point of homogenized MgY4.71La3.98 alloy (Fig. 5(b)). This structure has been seen all the way to the margins of the grain. In addition, at the grain boundaries, tiny, spherical objects have seen inside the grain. The spherical structure may be MgY, whereas the dendritic one is likely $LaMg_{12}$. At location E, it is possible to observe the presence of a La_2Mg_{17} phase characterized by cubic-like structures that extend from the grain border into the grain, with some of these structures have been located within the grain itself. The white contrast colored structure resembling a triangle at the F point and the dark gray contrast veined structures around this structure have attracted attention. The structure under consideration is believed to consist of intermetallic compounds, specifically $Mg_{12}La$ and Mg_2Y. Birbilis et al. [44] repoted increase in the volume percent intermetallic as a function of La alloying addition. The augmentation of the La based second phase might be related to the preferential segrega-

TABLE 2

Fig. 4(a)-(b) EDX phases (wt.%)

Points	Mg	Y	La	Zr
A	93.80	4.41	1.71	0.09
B	71.53	20.19	8.04	0.24
C	80.33	8.39	11.09	0.20
D	80.84	4.71	13.98	0.48
E	75.99	17.55	6.21	0.26
F	95.66	2.08	1.80	0.46

TABLE 3

Fig. 5(a)-(b) EDX phases (wt.%)

Points	Mg	Y	La	Zr
A	79.55	12.43	7.42	0.59
B	80.93	7.10	11.62	0.34
C	88.01	6.39	5.36	0.25
D	83.42	8.15	7.91	0.53
E	85.10	4.94	9.63	0.33
F	81.63	7.10	7.58	3.69

tion of La atoms at grain boundaries [45,46]. Y based spherical intermetalics at the solid-liquid interface during the solidification process led to the grain refinement and decrease in the dendride growth [47]. La is the dominant element in the microstructure of the sample alloyed with both La and Y elements, and the intermetallics generated at the grain boundaries get coarser when more alloying elements are added.

3.3. Hardness Test Results

TABLE 4 shows a comparison of MgY3.21La3.15 and MgY4.71La3.98 alloys in terms of hardness after casting and homogenization. In general, the hardness data show a rise following homogenization heat treatment. TABLE 4 shows that the hardest homogenized alloy is MgY3.21La3.15 (with a hardness of 93.70 HB), while the softest is as-cast MgY4.71La3.98 (with a hardness of 81.61 HB). It is believed that this is due to the evenly dispersed secondary phases.

TABLE 4

Hardness results of MgY3.21La3.15 and MgY4.71La3.98 alloys after casting and homogenization

Alloy	Hardness (HB)	
	As-Cast	Homogenized
MgY3.21La3.15	91.19	93.70
MgY4.71La3.98	81.61	87.37

The homogenization process led to an increase in hardness by evenly dispersing α-Mg and $Mg_{17}La_2$ eutectic phases along the grain boundaries, throughout distribution the fine particle within the structure (such as Mg_2Y, MgY, $Mg_{24}Y_5$, $Mg_{12}La$, $LaMg^3$) and solid solution strengthening [48]. Due to the augmentation of Y and La, the grain boundaries in the microstructure of the MgY4.71La3.98 alloy become larger, resulting in a decrease in its hardness [47,48]. With the exception of Refs. [43,49] that in many studies, up to 2% of both La and Y alloys were used. The complicated nature of these multicomponent systems may explain the change mechanisms in the attributes revealed in this study.

3.4. Tribological (Wear and Friction) Test Results

Fig. 6 illustrates the observed fluctuations in the weights of MgY3.21La3.15 and MgY4.71La3.98 alloys as a function of distance. Fig. 7 provides a comparative representation of the wear rates at a distance of 10000 meters. Additionally, Fig. 8 presents the friction coefficients recorded throughout the wear process. Alloys that undergo wear subsequent to the casting process indicate higher levels of weight loss, whereas alloys subjected to wear after the homogenization process have enhanced resistance to wear. MgY4.71La3.98 alloy was seen as the alloys with the weakest resistance to abrasion both after homogenization and after casting. The wear results support the hardness results and there is a parallelism in the results. After homogenization, MgY3.21La3.15 alloy was determined as the material with the least weight loss and the best wear resistance at the end of 10000 meters. Weight loss and wear rate of this material at the end of 10000 meters, respectively; 0.024 g and 2.44×10^{-6} g/Nm. The material with the highest weight loss and the worst wear resistance was observed in MgY4.71La3.98 alloy after casting. Weight loss and wear rate at the end of 10000 meters, respec-

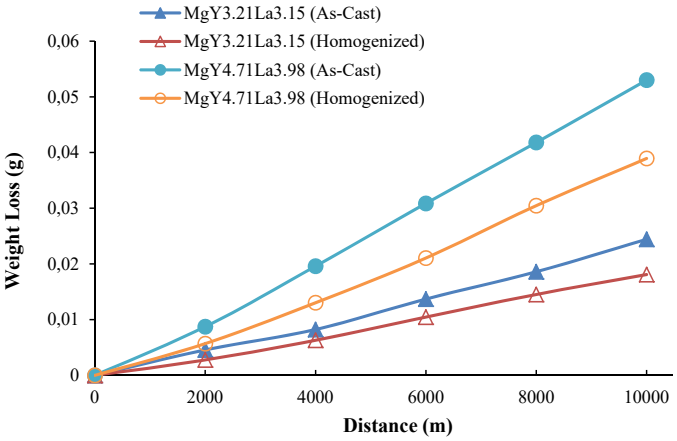

Fig. 6. Results of back and forth wear weight loss of MgY3.21La3.15 and MgY4.71La3.98 alloys after casting and homogenization

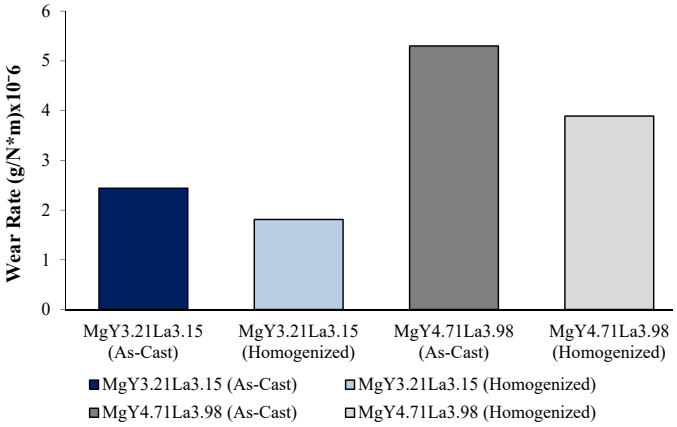

Fig. 7. Results of back and forth wear rates of MgY3.21La3.15 and MgY4.71La3.98 alloys after casting and homogenization

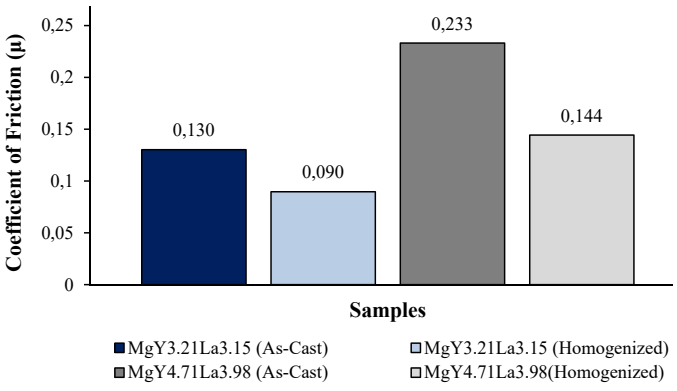

Fig. 8. Results of friction coefficient of MgY3.21La3.15 and MgY4.71La3.98 alloys after casting and homogenization

tively; 0.053 g and 5.30×10^{-6} g/Nm. Depending on these results, the friction coefficients during wear are also parallel and the material with the lowest friction coefficient is the MgY3.21La3.15 alloy after homogenization with a value of 0.090. Although the intermetallic precipitates become coarser and lower slightly the hardness with the increase in Y and La alloying elements [46]. The homogenization process led to, the improvement in wear behaviour can be attributed to the fact that the coarse phases formed at the grain boundaries during friction prevent weight loss.

The reason for the constant increase in the friction coefficient is explained based on the wear behavior and the condition of the contact surfaces. That is, the re-accumulation of some of the scraped particles on the wear surfaces as a result of wear in alloys creates resistance against movement during sliding. The increase in the coefficient of friction can be ascribed to the deformation encountered throughout the process of wear, as well as the heightened strength of the adhesive bond. Furthermore, it was observed that the surface hardness of the samples post-casting exhibited a notable decrease compared to the homogenized samples, resulting in a substantial increase in the breadth of the wear track. The augmentation of the contact area between the surfaces experiencing wear has led to a corresponding elevation in the friction coefficient.

According to SEM micrographs, it is seen that the effective wear mechanism is abrasive and adhesive wear types. As a result of the EDX analysis on the surface, a significant increase in the oxygen peak was observed, which clearly shows the existence of an oxidation wear mechanism. According to the wear micrographs obtained, it is seen that there are deposits caused by plastic deformation around the wear trace, abrasion grooves are formed, oxidized wear debris are formed and it is formed as a sharp-line scraping as a result of abrasive wear. In addition, the presence of traces showing the effectiveness of the three-body abrasion, that is, the abrasion mechanism of the abrasive particle by sliding, is observed in the abrasion. In addition, it was determined that the adhesive bonds formed between the abrasive surface and the matrix were broken as the experiment progressed and plastered back to the material surface due to their high deformation and load-bearing capabilities. Figs. 9(a) and 9(b) depict SEM micrographs of as cast MgY3.21La3.15 and MgY4.71La3.98 alloys. TABLE 5 presents the results of the Energy Dispersive X-ray (EDX) study conducted on the second phase, which exhibits different morphologies denoted as (A-D) in Fig. 9(a)-(b). Particles that detach from the matrix surface in the form of capillary fractures may be observed at point A in the as-cast MgY3.21La3.15 alloy, as depicted in Fig. 9(a). These particles are in the form of plastered on the matrix surface again with the pressure of the abrasive surface. Therefore, it is thought that the wear on the surface is of low order. At location B, the triangular debris on the surface becomes fully disengaged from the material's particular surface, resulting in a drop in the wear rate when re-adhesion to another surface takes place. At point C; the fragments that break off in the form of capillary cracks are plastered in a very small area on the material surface. In as cast MgY4.71La3.98 alloy (Fig. 9(b)), the situation at point A (Fig. 9(a)) is also dominant at point C. At location D, it is observed that a fragment that had been separated from the surface of the material had reattached itself to the worn surface. When the wear mechanism of as-cast MgY4.71La3.98 alloy is examined in general, it is seen that this situation is dominant on more material surfaces. Figs. 10(a) and 10(b) depict SEM micrographs of homogenized MgY3.21La3.15 and MgY4.71La3.98 alloys. TABLE 6 presents the results of the Energy Dispersive X-ray (EDX) study conducted on the second phase, which exhibits different morphologies as indicated by labels (A-D) in Fig. 10(a)-(b). In homogenized MgY3.21La3.15 alloy (Fig. 10(a)), at point A, swollen flakes in the form of sticky shells were observed due to adhesive wear. Particles separated from the surface due to this flaking are considered to support three-body abrasive wear. In general, except for the abrasive wear marks in Fig. 10(a), it is seen that the crust-shaped flakes are plastered on the material surface. The situation at point A dominates from that of point B in Fig. 10(a). It has been observed that the presence of oxidized wear residues is more evident in homogenized MgY4.71La3.98 alloy (Fig. 10(b)). The development of the oxide layer on the surface has resulted in a rise in

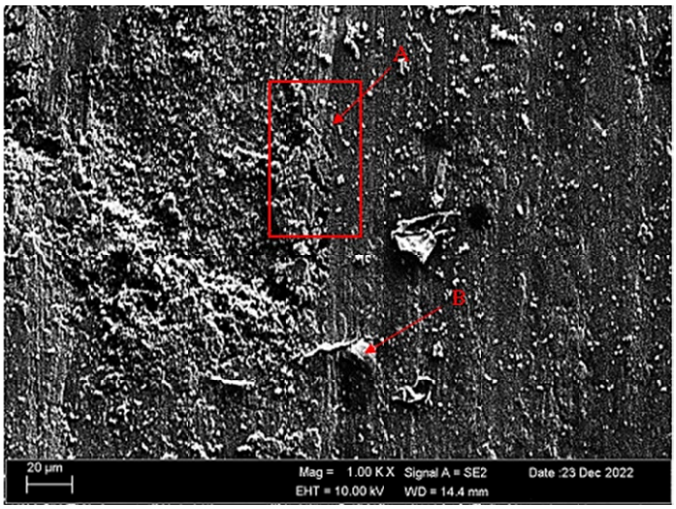

(a)

(b)

Fig. 9. SEM micrographs of alloys undergoing wear after casting: (a) MgY3.21La3.15 and (b) MgY4.71La3.98

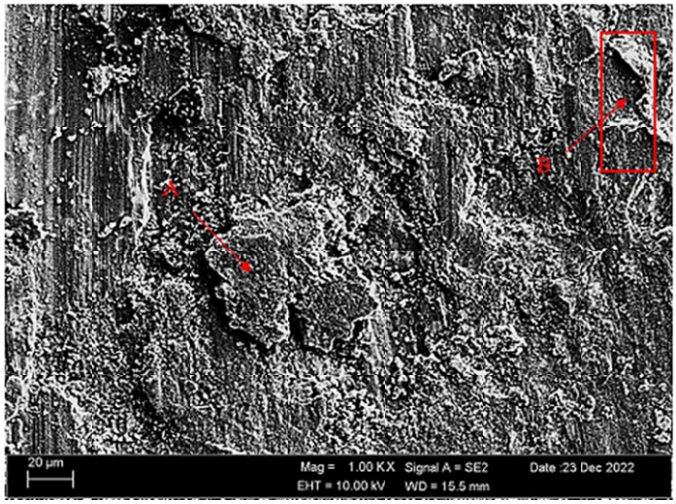

(a)

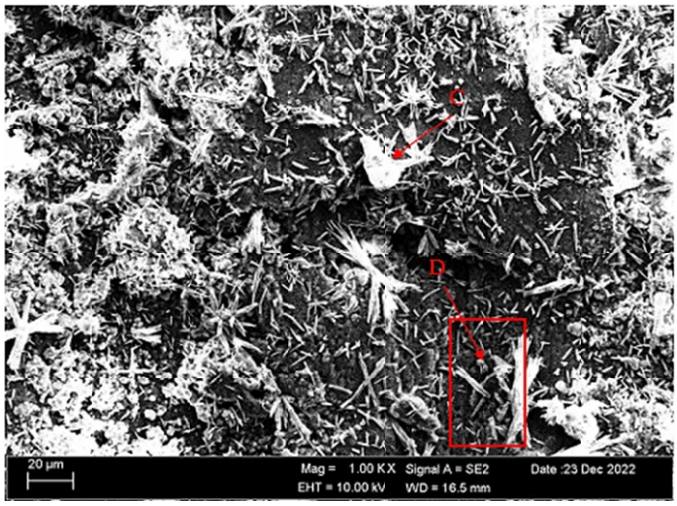

(b)

Fig. 10. SEM micrographs of alloys undergoing wear after homogenization: (a) MgY3.21La3.15 and (b) MgY4.71La3.98

TABLE 5

Fig. 9(a-b) EDX phases (wt.%)

Points	Mg	Y	La	Zr	Fe	O
A	53.11	3.09	2.14	0.35	—	41.33
B	53.82	2.64	1.62	0.25	0.01	41.68
C	60.62	2.33	1.37	0.08	0.07	35.54
D	53.14	2.55	2.85	0.16	0.10	41.21

TABLE 6

Fig.10(a-b) EDX phases (wt.%)

Points	Mg	Y	La	Zr	Fe	O
A	53.41	3.71	2.99	0.25	0.66	38.98
B	53.42	2.80	2.57	0.21	0.17	40.83
C	37.88	0.68	2.69	—	0.70	58.06
D	45.15	1.05	2.93	0.06	0.77	50.07

the magnitude of weight reduction. At point C, it is seen that the piece that broke off from the material surface is sticking to the material surface again. At the D point, it is seen that needle-shaped pieces from oxidized wear residues have adhered to the material surface.

4. Conclusions

In this work, tribological (wear and friction) characteristics in dry settings and microstructural characterizations of yttrium and lanthanum alloying elements added to magnesium in various quantities in casting and homogenization conditions were examined. And the following results have been given regarding this study:

- There are three-phase structures in microstructures. Included in this category are the eutectic compounds characterized by a reticular structure, as well as the α-Mg phases that exhibit lamellar morphology. The eutectic compounds were mostly observed in close proximity to the grain boundaries of the α-Mg crystals, whereas the lamellae-like phases exhibited a more uniform distribution inside the crystals. With a rise in La content, the eutectic phase consisting of α-Mg and $Mg_{17}La_2$ demonstrated a phenomenon of lamellae structure coarsening. The presence of yttrium resulted in an augmentation of dendrite-like phase structures and network structures at the grain boundaries. The process of homogenization has served to decrease the presence of lamellae-like phases inside the internal regions of α-Mg granules, hence has facilitated the even dispersion of alloy constituents over the entirety of the alloy system.
- While 93.70 HB value is the highest hardness of homogenized MgY3.21La3.15 alloy; With an HB value of 81.61, cast MgY4.71La is the alloy with the lowest hardness.
- According to their tribological properties, alloys that undergo wear subsequent to the casting process indicate higher levels of weight loss, whereas alloys subjected to wear after the homogenization process have enhanced resistance to wear. The homogenized MgY3.21La3.15 alloy is the material with the best wear resistance with a weight loss of 0.024 g and a wear rate of 2.44×10^{-6} g/Nm. Cast MgY4.71La3.98 alloy, on the other hand, is the material with the worst wear resistance with a weight loss of 0,053 g and a wear rate of 5.3×10^{-6} g/Nm. The friction coefficients during wear are also parallel and the material with the lowest friction coefficient is MgY3.21La3.15 alloy with a value of 0.090 after homogenization.

REFERENCES

[1] T. M. Pollock, Weight Loss with Magnesium Alloys. Science **328** (5981), 986-987 (2010).
DOI: https://doi.org/10.1126/science.1182848

[2] S. You, Y. Huang, K.U. Kainer, N. Hort, Recent research and developments on wrought magnesium alloys. J. Magnes. Alloy **5**, 239-253 (2017).
DOI: https://doi.org/10.1016/j.jma.2017.09.001

[3] S. Jin, H. Liu, R. Wu, F. Zhong, L. Hou, J. Zhang, Combination effects of Yb addition and cryogenic-rolling on microstructure and mechanical properties of LA141 alloy. Mater. Sci. Eng. A **788**, 139611 (2020).
DOI: https://doi.org/10.1016/j.msea.2020.139611

[4] W.J. Joost, P.E. Krajewski, Towards magnesium alloys for high-volume automotive applications. Scr. Mater. **128**, 107-112 (2017).
DOI: https://doi.org/10.1016/j.scriptamat.2016.07.035

[5] Q. Yang et al., Interphase boundary segregation induced phase transformation in a high-pressure die casting Mg-Al-La-Ca-Mn alloy. Mater. Des. **190**, 108566 (2020).
DOI: https://doi.org/10.1016/j.matdes.2020.108566

[6] K. Guan et al., Effects of samarium content on microstructure and mechanical properties of Mg–0.5Zn–0.5Zr alloy. J. Mater. Sci. Technol. **35**, 1368-1377 (2019).
DOI: https://doi.org/10.1016/j.jmst.2019.01.019

[7] N. Mo et al., Current development of creep-resistant magnesium cast alloys: A review. Mater. Des. **155**, 422-442 (2018).
DOI: https://doi.org/10.1016/j.matdes.2018.06.032

[8] A. Prasad, J. Jain, N.N. Gosvami, Effect of minor La addition on wear behaviour of Mg-10Dy alloy. Wear **486-487**, 204121 (2021).
DOI: https://doi.org/10.1016/j.wear.2021.204121

[9] F. Zhong et al., Effect of Y and Ce on the microstructure, mechanical properties and anisotropy of as-rolled Mg-8Li-1Al alloy. J. Mater. Sci. Technol. **39**, 124-134 (2020).
DOI: https://doi.org/10.1016/j.jmst.2019.04.045

[10] S. Jin et al., Mechanical properties, biodegradability and cytocompatibility of biodegradable Mg-Zn-Zr-Nd/Y alloys. J. Mater. Sci. Technol. **47**, 190-201 (2020).
DOI: https://doi.org/10.1016/j.jmst.2020.02.017

[11] R. Zhao, W. Zhu, J. Zhang, L. Zhang, J. Zhang, C. Xu, Influence of Ni and Bi microalloying on microstructure and mechanical properties of as-cast low RE LPSO-containing Mg–Zn–Y–Mn alloy. Mater. Sci. Eng. A **788**, 139594 (2020).
DOI: https://doi.org/10.1016/j.msea.2020.139594

[12] M. Janbozorgi, K. Karimi Taheri, A. Karimi Taheri, Microstructural evolution, mechanical properties, and corrosion resistance of a heat-treated Mg alloy for the bio-medical application. J. Magnes. Alloy. **7**, 80-89 (2019).
DOI: https://doi.org/10.1016/j.jma.2018.11.002

[13] J.F. Nie, Precipitation and Hardening in Magnesium Alloys. Metall. Mater. Trans. A **3**, 3891-3939 (2012).
DOI: https://doi.org/10.1007/s11661-012-1217-2

[14] D. Liu, D. Yang, X. Li, S. Hu, Mechanical properties, corrosion resistance and biocompatibilities of degradable Mg-RE alloys: A review. J. Mater. Res. Technol. **8**, 1538-1549 (2019).
DOI: https://doi.org/10.1016/j.jmrt.2018.08.003

[15] D.H. StJohn, P. Cao, M. Qian, M.A. Easton, A New Analytical Approach to Reveal the Mechanisms of Grain Refinement. Adv. Eng. Mater. **9**, 739-746 (2007).
DOI: https://doi.org/10.1002/adem.200700157

[16] D.H. StJohn, M. Qian, M.A. Easton, P. Cao, Z. Hildebrand, Grain refinement of magnesium alloys. Metall. Mater. Trans. A **36**, 1669-1679 (2005).
DOI: https://doi.org/10.1007/s11661-005-0030-6

[17] C.H. Caceres, G.E. Mann, J.R. Griffiths, Grain size hardening in Mg and Mg-Zn solid solutions. Metall. Mater. Trans. A Phys. Metall. Mater. Sci. **42**, 1950-1959 (2011).
DOI: https://doi.org/10.1007/s11661-010-0599-2

[18] C.H. Cáceres, W.J. Poole, A.L. Bowles, C.J. Davidson, Section thickness, macrohardness and yield strength in high-pressure diecast magnesium alloy AZ91. Mater. Sci. Eng. A **402**, 269-277 (2005).
DOI: https://doi.org/10.1016/j.msea.2005.04.024

[19] D. Zhang et al., Improvement on both strength and ductility of Mg−Sm−Zn−Zr casting alloy via Yb addition. J. Alloys Compd. **805**, 811-821 (2019).
DOI: https://doi.org/10.1016/j.jallcom.2019.07.094

[20] K. Wang et al., Achieving enhanced mechanical properties in Mg-Gd-Y-Zn-Mn alloy by altering dynamic recrystallization behavior via pre-ageing treatment. Mater. Sci. Eng. A **790**, 139635 (2020).
DOI: https://doi.org/10.1016/j.msea.2020.139635

[21] Y. Li, C. Yang, X. Zeng, P. Jin, D. Qiu, W. Ding, Microstructure evolution and mechanical properties of magnesium alloys containing long period stacking ordered phase. Mater. Charact. **141**, 286-295 (2018).
DOI: https://doi.org/10.1016/j.matchar.2018.04.044

[22] J. Zhang, S. Liu, R. Wu, L. Hou, M. Zhang, Recent developments in high-strength Mg-RE-based alloys: Focusing on Mg-Gd and Mg-Y systems. J. Magnes. Alloy. **6**, 277-291 (2018).
DOI: https://doi.org/10.1016/j.jma.2018.08.001

[23] S.M. Ashrafizadeh, R. Mahmudi, A.R. Geranmayeh, A comparative study on the effects of Gd, Y and La rare-earth elements on the microstructure and creep behavior of AZ81 Mg alloy. Mater. Sci. Eng. A **790**, 139712 (2020).
DOI: https://doi.org/10.1016/j.msea.2020.139712

[24] L.L. Rokhlin, Magnesium Alloys Containing Rare Earth Metals: Structure and Properties. (Taylor & Francis, 2003).

[25] M. Socjusz-Podosek, L. Lityńska, Effect of yttrium on structure and mechanical properties of Mg alloys. Mater. Chem. Phys. **80**, 472-475 (2003).
DOI: https://doi.org/10.1016/S0254-0584(02)00549-7

[26] K. Luo, L. Zhang, G. Wu, W. Liu, W. Ding, Effect of Y and Gd content on the microstructure and mechanical properties of Mg–Y–RE alloys. J. Magnes. Alloy. **7**, 345-354 (2019).
DOI: https://doi.org/10.1016/j.jma.2019.03.002

[27] L. Chang, J. Guo, X. Su, Effect of Y on microstructure evolution and mechanical properties of Mg−4Li−3Al alloys. Trans. Nonferrous Met. Soc. China **31**, 3691-3702 (2021).
DOI: https://doi.org/10.1016/S1003-6326(21)65757-6

[28] H. Zengin, Y. Turen, H. Ahlatci, Y. Sun, Microstructure, mechanical properties and corrosion resistance of as-cast and as-extruded Mg–4Zn–1La magnesium alloy. Rare Met. **39**, 909-917 (2020).
DOI: https://doi.org/10.1007/s12598-018-1045-7

[29] Y.F. Liu, X.J. Jia, X.G. Qiao, S.W. Xu, M.Y. Zheng, Effect of La content on microstructure, thermal conductivity and mechanical properties of Mg–4Al magnesium alloys. J. Alloys Compd. **806**, 71-78 (2019).
DOI: https://doi.org/10.1016/j.jallcom.2019.07.267

[30] Y. Du, M. Zheng, X. Qiao, W. Peng, B. Jiang, Effect of La addition on the microstructure and mechanical properties of Mg–6 wt% Zn alloys. Mater. Sci. Eng. A **673**, 47-54 (2016). DOI: https://doi.org/10.1016/j.msea.2016.07.022

[31] G. Yarkadaş, L.C. Kumruoğlu, S. Özarslan, H. Şevik, Effect of Lanthanum on mechanical and wear properties of high-pressure die-cast Mg-3Al-3Sn-3Sb alloy. Mater. Test. **63**, 85-91 (2021). DOI: https://doi.org/10.1515/mt-2020-0012

[32] M. Nouri, X. Sun, D.Y. Li, Beneficial effects of yttrium on the performance of Mg–3%Al alloy during wear, corrosion and corrosive wear. Tribol. Int. **67**, 154-163 (2013). DOI: https://doi.org/10.1016/j.triboint.2013.07.012.

[33] A. Zafari, H.M. Ghasemi, R. Mahmudi, Effect of rare earth elements addition on the tribological behavior of AZ91D magnesium alloy at elevated temperatures. Wear **303**, 98-108 (2013). DOI: https://doi.org/10.1016/j.wear.2013.02.016

[34] S.M. Banijamali, M. Shariat Razavi, Y. Palizdar, S. Najafi, A. Sheikhani, H. Torkamani, Experimental and Simulation Study on Wear Behavior of ZK60 Alloy with 3 wt.% Yttrium Addition. J. Mater. Eng. Perform. **31**, 4721-4734 (2022). DOI: https://doi.org/10.1007/s11665-022-06585-y

[35] K. Hamdy, Investigation of the abrasion resistance of aluminum copper magnesium alloy. J. Egypt. Soc. Tribol. **19**, 19-27 (2022).

[36] F. Findik, Latest progress on tribological properties of industrial materials. Mater. Des. **57**, 218–244 (2014).

[37] X. Zhang, K. Zhang, Z. Wu, Effect of Homogenization Treatment on the Corrosion Behavior and Mechanism of Mg-Y Alloys. J. Wuhan Univ. Technol. Mater. Sci. Ed. **35**, 635-652 (2020).

[38] H. Okamoto, H. La-Mg (Lanthanum-Magnesium). JPEDAV **27**, 550 (2006). DOI: https://doi.org/10.1361/154770306X136647

[39] R.S. Campos, D. Höche, C. Blawert, K.U. Kainer, Influence of Lanthanum concentration on the Corrosion Behaviour of Binary Mg-La Alloys. Magnesium Technology **2011**, 507-–511 (2011). DOI: https://doi.org/10.1007/978-3-319-48223-1_94

[40] X. Liu, D. Shan, Y. Song, E.H. Han, Influence of yttrium element on the corrosion behaviors of Mg–Y binary magnesium alloy. J. Magnes. Alloys **5**, 26-34 (2017). DOI: https://doi.org/10.1016/j.jma.2016.12.002

[41] X. Zhang, K. Zhang, Z. Wu, Effect of Homogenization Treatment on the Corrosion Behavior and Mechanism of Mg-Y Alloys. J. Wuhan Univ. Technol. Sci. Ed. **35**, 635-652 (2020). DOI: https://doi.org/10.1007/s11595-020-2301-x

[42] H. Guo, S. Liu, L. Huang, D. Wang, Y. Du, M. Chu, Thermal conductivity of As-cast and annealed Mg-RE binary alloys. Metals (Basel). **11**, (2021). DOI: https://doi.org/10.3390/met11040554

[43] M. Sugamata, S. Hanawa, J. Kaneko, Structures and mechanical properties of rapidly solidified Mg-Y based alloys. Mater. Sci. Eng. A **226-228**, 861-866 (1997). DOI: https://doi.org/10.1016/S0921-5093(97)80089-5

[44] N. Birbilis, M.A. Easton, A.D. Sudholz, S.M. Zhu, M.A. Gibson, On the corrosion of binary magnesium-rare earth alloys. Corr. Sci. **51**, 683-689 (2009). DOI: https://doi.org/10.1016/j.corsci.2008.12.012

[45] A. Prasad, H. Vashishtha, S.S. Singh, N.N. Gosvami, J. Jain, La containing Mg alloy for enhanced corrosion at elevated temperatures in ethylene glycol media. Corr. Sci. **205**, (2022). DOI: https://doi.org/10.1016/j.corsci.2022.110446.

[46] M.M. Janet, C. Josh, A.L. Alan, Towards high strength cast Mg-RE based alloys: Phase diagrams and strengthening mechanisms. J. Mag. Alloys **10**, 1401-1427 (2022). DOI: https://doi.org/10.1016/j.jma.2022.03.008

[47] H. Zengin, Y. Turen, Effect of Y addition on microstructure and corrosion behavior of extruded Mg–Zn–Nd–Zr alloy, J. Mag. Alloys **8**, 640-653 (2020). DOI: https://doi.org/10.1016/j.jma.2020.06.004

[48] S. Tekumalla, S. Seetharaman, A. Almajid, Gupta, M. Mechanical Properties of Magnesium-Rare Earth Alloy Systems: A Review. Metals **5**, 1-39 (2015). DOI: https://doi.org/10.3390/met5010001

[49] B.L. Wu, Y.H. Zhao, X.H. Du, Y.D. Zhang, F. Wagner, C. Esling, Ductility enhancement of extruded magnesium via yttrium addition,. Mater. Sci. Eng. A **527**, 4334-4340 (2010). DOI: https://doi.org/10.1016/j.msea.2010.03.054